Research paper

Free-standing and flexible Cu/Cu$_2$O/CuO heterojunction net: A novel material as cost-effective and easily recycled visible-light photocatalyst

Heping Li *, Zhen Su, Sanyuan Hu, Youwei Yan *

State Key Laboratory of Materials Processing and Die & Mould Technology, School of Materials Science and Engineering, Huazhong University of Science and Technology, Wuhan 430074, PR China

ARTICLE INFO

ABSTRACT

Facing the worldwide deepening water-shortage and water-contamination crises, developing visible-light photocatalysts for water purification is an urgent need. However, the present photocatalysts are mostly in form of powders and nanoparticles, which make the recovery inevitably depend on expensive separation processes. The great challenge of photocatalyst recovery severely limits their industry applications. Herein, a new kind of free-standing and flexible visible-light photocatalyst that can be easily recycled is developed for the first time. Cu/Cu$_2$O/CuO heterojunction net is successfully fabricated by one-step calcination in air using low-cost Cu net as the matrix. The mixing narrow band gaps of the Cu/Cu$_2$O/CuO heterojunction ensure its wide absorption band in visible region and effective electron/hole separation, and consequently lead to markedly photocatalytic activity under visible light irradiation. In addition, a large number of CuO nanowires growing on the heterojunction surface provide high specific surface area, expose abundant active sites for photocatalysis, and thus guarantee its high photocatalytic efficiency. More importantly, the Cu/Cu$_2$O/CuO photocatalyst possesses flexible property for recovery, which is a significant advance in comparison with the previously reported photocatalysts. With a marvelous combination of low cost, facile fabrication, visible-light response, and easy recycling characteristic, this newly developed photocatalyst is expected to have great potential applications in water crises.

1. Introduction

In these years, human beings have faced the worldwide deepening water-shortage and water-contamination crises. Water contamination by organic pollutants not only aggravates the water-shortage situation but also causes an inevitable public health problem. As estimated, four billion people have no clean water to use, and millions of people die of water borne diseases each year [1]. Therefore, accessible techniques for removing organic pollutants from water are urgently needed.

As the photocatalysts can generate highly oxidizing species in water under solar irradiation and consequently mineralize organic pollutants through oxidation reactions, photocatalysis has been recognized as one of the most promising solutions to these water crises [2]. During the past decades, titanium dioxide, a dominated and famous photocatalyst, has received most of the attention because of its high photocatalytic efficiency [3–6]. However, due to its wide band gap (~3.2 eV), TiO$_2$ can only be activated by UV light irradiation, which just accounts for 5% of the solar energy. With such a drawback, the application of TiO$_2$ in water purification is thus greatly hindered. In this case, searching for new visible-light photocatalysts is highly desirable.

Nowadays, the materials with a narrow band gap (especially Bi-based oxides), attract increasing attention for their visible-light absorption. BiFeO$_3$ [7], Bi$_2$MoO$_6$ [8], BiWO$_6$ [9], BiVO$_4$ [10], and Bi$_3$NbO$_7$ [11] have emerged as potential visible-light photocatalysts. Successful degradation of organic pollutants such as acetone, phenol, aqueous ammonia, methylene blue, and rhodanmine B by these emerging photocatalysts under visible light illumination has been reported. Despite the significant advances, the single phase visible-light photocatalysts with a narrow band gap still suffer from poor photocatalytic activity, which is ascribed to their high electron/hole recombination [12].

To enhance the visible-light photocatalytic efficiency, heterojunction materials have been proposed and developed as promising alternatives. Consisting of two or even more phases with

---

* Corresponding authors.
E-mail addresses: liheping@hust.edu.cn (H. Li), yanyw@hust.edu.cn (Y. Yan).

different band gaps, heterojunction photocatalysts can broaden the light absorption edge to the visible region and meanwhile possess high transfer efficiency of photogenerated charges [13]. This marvelous combination of wide absorption band and effective electron/hole separation will enable heterojunction photocatalysts to exhibit excellent visible-light photocatalytic activity. Novel heterostructures have been exploited with outstanding photocatalytic performance toward removing organic pollutants, such as $Ag/AgBr/AgVO_4$, $Ag/AgCl/BiVO_4$, $Ag/AgCl/g-C_3N_4$, $Ag/Ag_3PO_4/g-C_3N_4$, $AgI/AgIO_3$, $Bi_7O_9I_3/AgI/AgIO_3$, $Bi_7O_9I_3/AgI$, and $Ag_2O/Ag_3VO_4/AgVO_3$ [14–19]. However, most of these materials contain silver (a kind of noble metal), whose high cost will certainly limit their large-scale use. Moreover, to realize applications of heterojunction photocatalysts, two vital issues are challenging but needed to be addressed: facile fabrication and easy recycling. As reported in the literatures [20–22], the heterojunction photocatalysts were generally fabricated by complex procedures involving multiple steps. The tedious fabrication process seriously limited their actual use. In addition, the resulted photocatalysts were usually in form of powders and nanoparticles, and thus, the photocatalysis had to be used with their suspension. This leaded to the difficult recovery of the catalyst, which involved expansive separation processes [23]. So far, easily recycled visible-light photocatalysts have been unrealized. In this context, exploiting low-cost materials by facile fabrication strategies and developing easily recycled visible-light photocatalysts is expected for water purification.

Copper-oxide compounds (including CuO, Cu_3O_4, and Cu_2O) have prominent superiorities such as high abundance, low cost, facile fabrication, and nontoxicity of the elements [24]. Moreover, due to their small band gap energies, copper oxides can absorb vast majority of solar spectrum [25]. Currently, there is much interest on copper oxides with respect to photocatalytic H_2 production and solar-cell applications [26–29]. Cu_xO-TiO_2 hybrids have been successfully fabricated both for high-performance dye-sensitized solar cells and for photocatalytic H_2 generation [26,27]. Zhang et al. obtained the $Cu/Cu_2O/CuO/TiO_2$ multi-heterojunction nanofibers with a greatly enhanced photoactivity in the case of H_2 generation by photocatalytic decomposition of HCOOH [28]. Yang et al. prepared Cu_2O/CuO bilayered composites, which exhibited a high activity toward photoelectrochemical hydrogen evolution reaction [29]. Even though CuO structures with various morphologies have been investigated as photocatalysts for water purification, their photocatalytic degradation efficiency directly depended on the presence of H_2O_2 [30–32]. To enhance the photocatalytic activity of CuO, CuO/Co_3O_4 and CuO/graphene have been synthesized [33,34]. Despite these advances, however, there is still a lot of room for improvement. Until now, few attentions have been paid on the preparation of free-standing photocatalysts, and hence easily recycled visible-light photocatalysts are still out of reach.

In view of this, we developed $Cu/Cu_2O/CuO$ heterojunction net as a new type of photocatalyst for the first time. Copper is a relatively abundant and inexpensive material. Using a commercial Cu net as the matrix, a free-standing and flexible $Cu/Cu_2O/CuO$ heterojunction net was facilely fabricated by one-step annealing method. Intriguingly, the obtained $Cu/Cu_2O/CuO$ heterojunction exhibited considerable photocatalytic activity toward the degradation of rhodanmine B (RhB) under an ordinary table lamp irradiation, which indicates its potential use as cost-efficient visible-light photocatalyst. Furthermore, the free-standing and flexible characteristics of the $Cu/Cu_2O/CuO$ heterojunction net allowed for easy recycling during the photocatalysis. Considering its low-cost, facile fabrication, visible-light response, and easy recycling characteristic, the $Cu/Cu_2O/CuO$ heterojunction net is expected to facilitate the applications of photocatalysts in water purification.

2. Experimental

2.1. Fabrication of $Cu/Cu_2O/CuO$ heterojunction net

Commercial Cu nets were purchased from Shijiazhuang HangXu Metal Products Co., Ltd. (China) with purity of 99.96%. The diameter of a single Cu wire is $50\,\mu m$. The Cu nets were cut in $3.2 \times 3.2\,cm^2$ pieces. These pieces were immersed in HCl solution (1 mol/L) and then rinsed by ethanol to remove surface native oxide layer. After drying at room temperature, the sample was immediately annealed at $500\,°C$ in air with a heating rate of $5\,°C\,min^{-1}$. The $Cu/Cu_2O/CuO$ heterojunction net was thus obtained.

2.2. Characterization

The crystallinity and microstructure of the samples was determined by X-ray diffraction (XRD, X'pert PRO, PANalytical B.V., Netherlands) and Field transmission electron microscopy (FTEM, Tecnai G2 F30, FEI, Netherlands). Field emission scanning electron microscopy (FESEM, NovaNano SEM 450, FEI, Netherlands) was used to observe the sample morphology. X-ray photoelectron spectroscopy (XPS, AXIS-ULTRA DLD-600W, Kratos) was also performed for composition determination.

2.3. Photocatalytic performance measurements

The visible-light photocatalytic activity of the sample was evaluated by the degradation of Rhodamine B (RhB) under irradiation of an ordinary table lamp (27 w, the power density was approximately $138\,w/m^2$, $\lambda = 400–750\,nm$). At the beginning, the sample was immersed in the RhB solution (initial concentration of 2.5×10^{-5} mol/L, 10 mL) in an open beaker, and was then kept in dark for 30 min to achieve adsorption-desorption equilibrium of RhB with the sample. Afterwards, the RhB solution containing the sample was irradiated by the table lamp. During the irradiation, the concentration of RhB was followed by their absorption at 554 nm, which was measured using a UV–vis spectrophotometer (Shimadzu, UV3600).

3. Results and discussion

The $Cu/Cu_2O/CuO$ heterojunction net was fabricated simply by annealing the Cu net in air at $500\,°C$. As shown in Fig. 1a, the commercial Cu net with a yellow color is woven of micron-sized Cu wires, whose diameter is approximately $50\,\mu m$. After annealing, the sample was unbroken, but its color was turned into dark gray. A large number of nanowires grew uniformly on the sample surface, as observed in its SEM image. Fig. 1b shows the XRD patterns of the samples annealed at $500\,°C$ for 3 h and 9 h, respectively. The emerging diffraction peaks were well indexed to cubic Cu, cubic Cu_2O, and monoclinic CuO. It is noted that the CuO content in the sample clearly increased with the annealing time increasing. However, no other phases were detected. The XRD results indicated that the resulted samples were composed of a $Cu/Cu_2O/CuO$ heterojunction structure. The similar structure could also be obtained at $450\,°C$ with a lower content of Cu_2O and CuO (Fig. S1). The following composition characterizations, which are detailed in the latter section, demonstrated the $Cu/Cu_2O/CuO$ heterojunction was probable a Cu net coated by Cu_2O layer with CuO nanowires growing vertically on the surface. The formation of this unique heterojunction net is schematically depicted in Fig. 1c. The mechanism for forming $Cu/Cu_2O/CuO$ is proposed as follows. When copper was annealed in air, Cu_2O was firstly formed on its surface, protecting the inner Cu from being further oxidized and simultaneously serving as a precursor to the growth of CuO. CuO nanowires then grew vertically on the Cu_2O surface based on a vapor-solid mechanism [35,36]. The
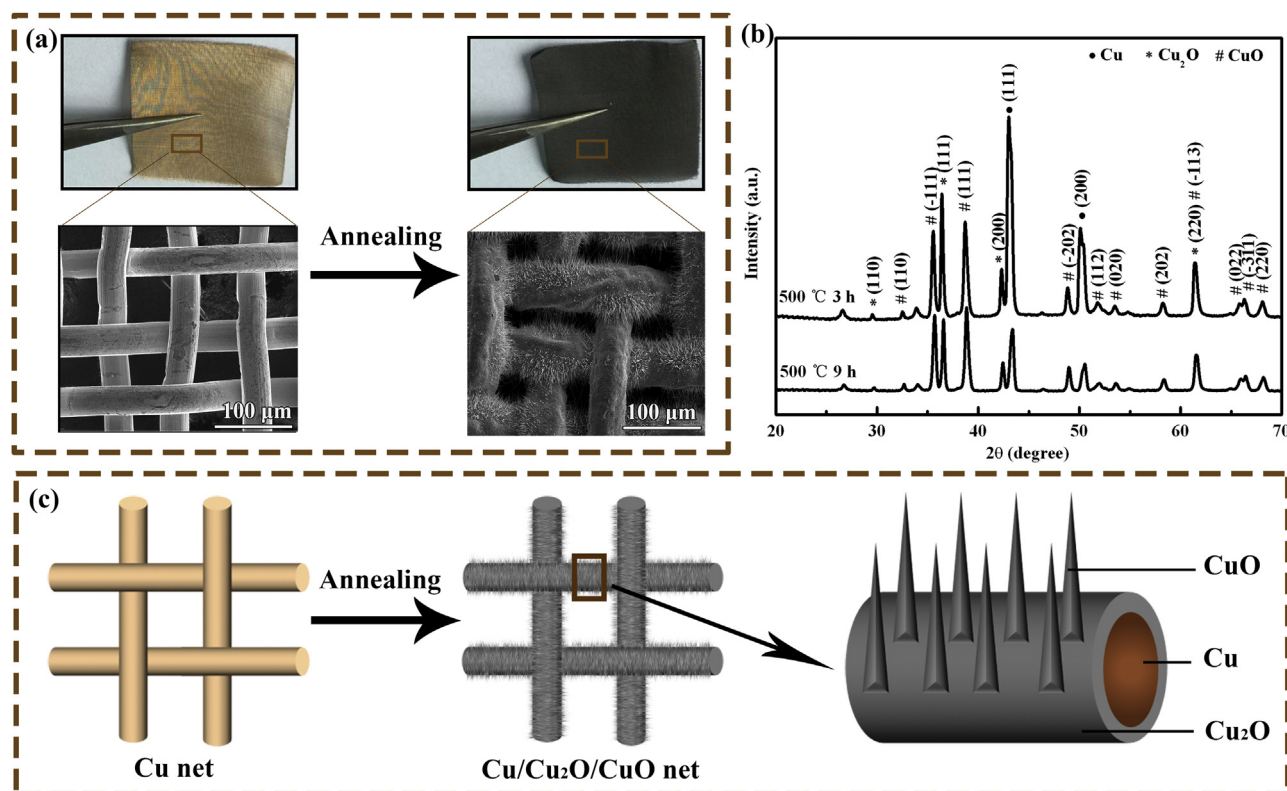
Fig. 1. (a) Morphology of the Cu net and the Cu/Cu$_2$O/CuO heterojunction net. (b) XRD patterns of the Cu/Cu$_2$O/CuO heterojunction net annealed at 500 °C. (c) a schematic illustration for fabricating Cu/Cu$_2$O/CuO heterojunction.

following are the corresponding reactions for producing Cu$_2$O and CuO:

$$4Cu + O_2 \rightarrow 2Cu_2O \tag{1}$$

$$2Cu_2O + O_2 \rightarrow 4CuO \tag{2}$$

The slow rate of reaction (2) ensured a relatively low CuO vapor pressure in the reaction chamber, and thus allowed for uniform CuO nanowire arrays growing on the Cu$_2$O surface in a continuous growth mode [35]. Finally, after the oxidation annealing, a Cu/Cu$_2$O/CuO heterojunction net was obtained as shown in Fig. 1c.

Fig. 2 shows SEM images of the sample both before and after annealing. The original Cu net had a relatively smooth surface (Fig. 2a–c). Interestingly, the surface became rather rough after annealing, which seemed like the bark of a tree. On the rough surface, vertical nanowire arrays grew uniformly with a length of several micrometers (Fig. 2d–f). In addition, as the annealing time increased, much denser nanowire arrays with an increasing length were observed (Fig. 2g–i).

The TEM characterization was carried out to give a further insight into the microstructure of the sample after annealing. Both the surface component and the growing nanowires were peeled off from the annealed net for TEM characterization. Fig. 3a shows the TEM image of a nanowire growing on the net surface, whose diameter was 130 nm. In its high-resolution TEM image (Fig. 3b), the crystal lattices were calculated to be 2.53 Å and 2.75 Å, agreeing well with monoclinic CuO (002) and (110), respectively. The corresponding TEM diffraction pattern of the nanowire also displayed a crystallized CuO structure (Fig. 3c). These results revealed that the vertical arrays growing on the net surface were CuO nanowires. The surface component of the net is presented in the inset of Fig. 3d. The spacing d of 2.46 Å was in accord with the lattice fringe of cubic Cu$_2$O (111). Its TEM diffraction pattern was indicative of the polycrystalline Cu$_2$O and CuO structure (Fig. 3e). The presence of

CuO was probably attributed to the unremoved root of the CuO nanowire, which grew on the Cu$_2$O layer and adhered firmly to the net surface. Based on the TEM analysis, it was speculated that during the annealing process Cu$_2$O layer formed on the original Cu net surface, and subsequently, CuO nanowire arrays grew vertically on the Cu$_2$O layer. This is in a good agreement with the aforementioned XRD results, which were indicative of the resulted Cu/Cu$_2$O/CuO heterojunction structure.

The chemical states of Cu and O atoms in the heterojunction were further detected by X-ray photoelectron spectroscopy (XPS) experiments. As shown in Fig. 4a, the Cu 2p$_{3/2}$ signal is consisted of four peaks (Fig. 4a). Among them, the peak located at 933.3 eV was ascribed to Cu^{1+} [37], verifying the existence of Cu$_2$O. The other peak located at 934.7 eV and two satellite peaks (941.6 and 944.0 eV) were corresponding to Cu^{2+} [38–40], which demonstrated the existence of CuO. The copper species were additionally distinguished by the Auger spectra (inset of Fig. 4a). The peaks located at 568.2, 568.5, and 569.5 eV were assigned to Cu, Cu^{2+}, and Cu$^+$, respectively [41,42]. Fig. 4b shows the O 1 s signal of the heterojunction. According to the literature, the peak at 529.9 eV belonged to the lattice oxygen from both Cu$_2$O and CuO phases [43]. The other peak at 531.6 eV related to surface hydroxyl group [44].

Fig. 5 presents the UV–vis diffuse reflectance spectra of the Cu/Cu$_2$O/CuO heterojunction. The Cu/Cu$_2$O/CuO extended the absorption edge to 715 nm on account of the low band gap of both Cu$_2$O and CuO. The band gap of the heterojunction was obtained from UV–vis spectra using the following equation [45,46]:

$$(\alpha h\nu)^{1/2} = A(h\nu - E_g) \tag{3}$$

where α is the absorption coefficient, $h\nu$ is the energy of photon, A is a constant, and E_g is the optical band gap energy. The obtained band gap energy of Cu/Cu$_2$O/CuO was 1.68 eV. From the XPS-VB shown
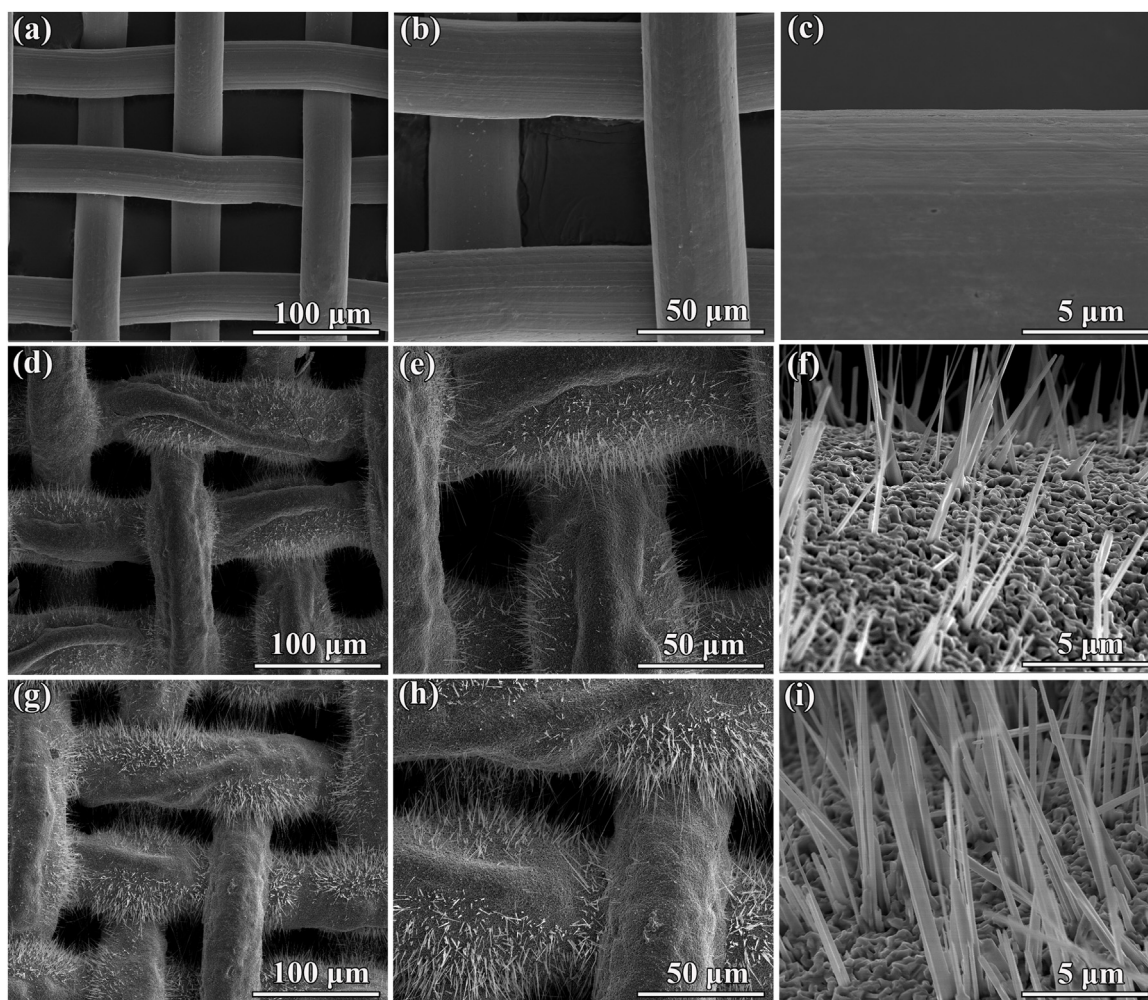
Fig. 2. SEM images of the sample annealed for different time: (a–c) 0 h; (d–f) 3 h; (g–i) 9 h.

in Fig. S2, the observed VB position of Cu/Cu$_2$O/CuO heterojunction was 0.56 eV [47].

The visible-light photocatalytic activity of the Cu/Cu$_2$O/CuO heterojunction net was evaluated with the degradation of RhB. Before the photocatalytic activity study, the adsorption-desorption equilibrium of RhB and the blank experiment were carried out with the results shown in Fig. 6d–e. No appreciable reduction in the dye was observed in these conditions, which demonstrated that the following degradation of RhB could only be caused by the photocatalytic degradation reaction under visible light. The photocatalytic tests were performed using a setup schematically illustrated in Fig. 6a. An ordinary table lamp with a power of 27 w (λ = 400–750 nm, the power density was approximately 138 w/m^2) was employed as the irradiation light source. To reach the adsorption equilibrium, the Cu/Cu$_2$O/CuO heterojunction net was firstly immersed in the RhB solution in the dark for 30 min. After that, the lamp was turned on and the photocatalytic degradation reaction took place. During the photocatalytic test, the RhB concentration was followed by the UV–vis spectroscopy, as recorded in Fig. 6b. As the photocatalysis proceeded, the RhB concentration apparently dropped due to the effective degradation reaction caused by the Cu/Cu$_2$O/CuO heterojunction. Degradation of RhB made the solution color gradually become light (Fig. 6c). The decreasing RhB concentration was plotted as a function of the photocatalysis time in Fig. 6d–e. Compared with the sample annealed for 3 h, RhB was removed more quickly by the sample annealed for 9 h. It is worth to mention that the degradation rate constant of the sample annealed for 9 h was

0.012 min^{-1}, which was almost twice that of the sample annealed for 3 h. According to the XRD spectra and SEM images, the increase in the degradation rate was mainly caused by the denser CuO nanowire arrays growing on the net surface. These proliferated CuO nanowires could offer a larger specific surface area, enhance the light absorption, and therefore improved the photocatalytic activity. The sample was also annealed at 500 °C for 12 h to give more insight into the effect of annealing time on the heterojunction composition and property. From its SEM images (Fig. S3a–c), the number of CuO nanowire arrays significantly increased with the annealing time increasing from 9 h to 12 h. This observation was in accord with the XRD data (Fig. S3d), where the increasing ratio of CuO/Cu$_2$O was displayed. Even though the increase in annealing time was beneficial for the growth of CuO nanowires, the Cu$_2$O layer partly peeled off and cracks were also observed on the heterojunction surface (Fig. S3a–b). As a result, the sample annealed for 12 h was relatively fragile due to the more powerful oxidation of Cu framework (Fig. S3e–f). This fragile nature will be unfavourable for photocatalyst recovery after photocatalysis. When annealed at 450 °C, the photocatalytic activity of the catalyst was clearly decreased due to the decreasing Cu$_2$O and CuO contents (Fig. S4, Fig. S5). Therefore, the optimum annealing condition for fabricating free-standing Cu/Cu$_2$O/CuO heterojunction was at 500 °C for 9 h. The considerable photocatalytic activity reached suggests great potential applications of Cu/Cu$_2$O/CuO as visible-light photocatalyst.
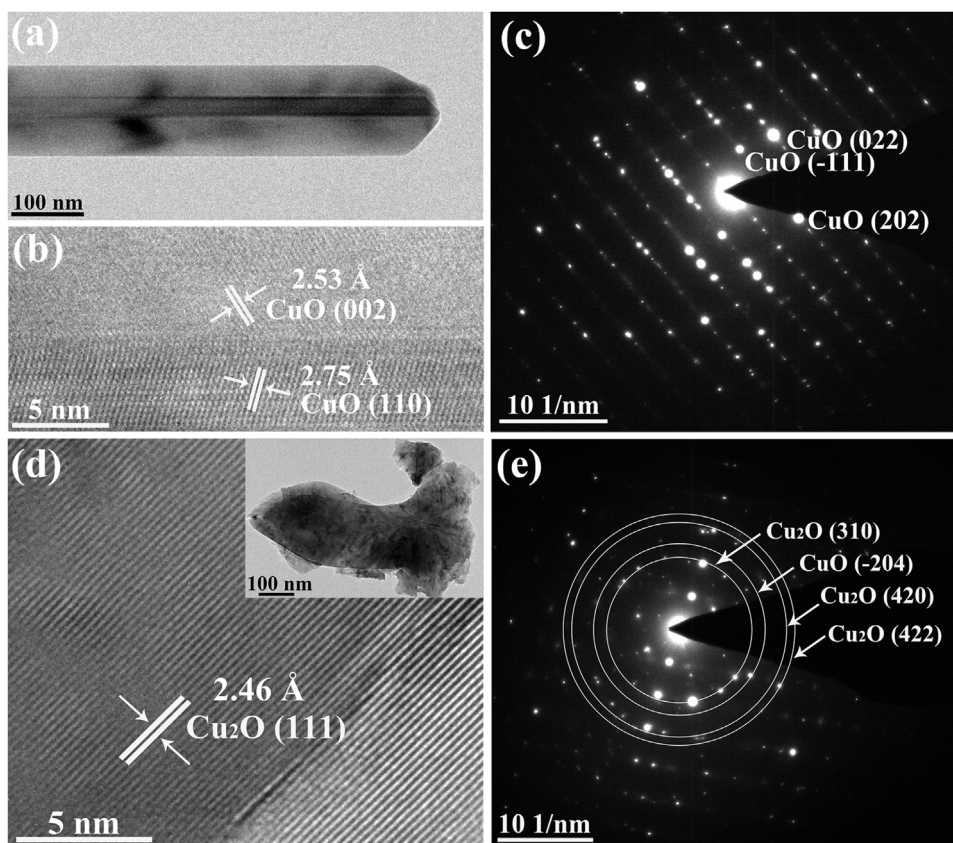
Fig. 3. (a, b) TEM images and (c) SAED pattern of an individual CuO nanowire. (c) TEM image and (d) SAED pattern of a Cu$_2$O flake.
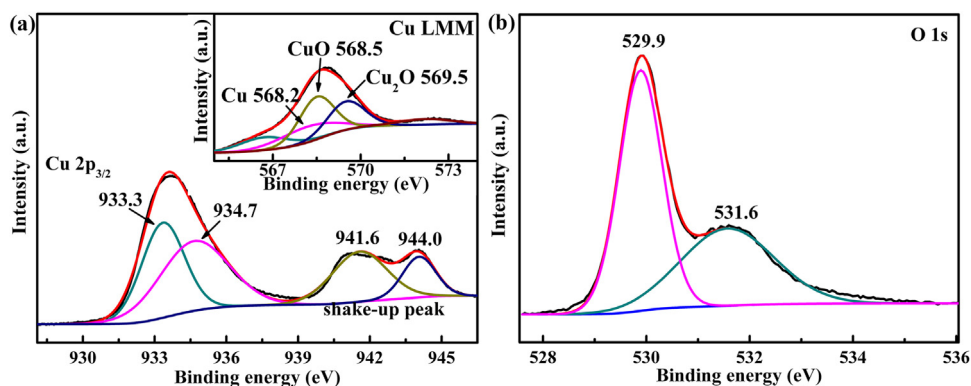

Fig. 4. XPS spectra of the Cu/Cu$_2$O/CuO heterojunction net: (a) Cu 2p$_{3/2}$ XPS spectra, Auger spectra of Cu (inset); (b) O 1 s XPS spectra.

To further evaluate the potential of this new material for photocatalysis, we have tested the repeatability of the Cu/Cu$_2$O/CuO heterojunction net by applying three photocatalysis operations. Fig. 6f shows the recorded degradation data from three-cycle tests. It was intriguing to find that the photocatalytic degradation behavior of the sample was repeatable. The degradation rate constants for the three cycles were 0.012, 0.010, and 0.009 min^{-1}, respectively. In the third cycles, the degraded RhB proportion slightly decreased under the same photocatalysis condition. After the photocatalysis tests, the composition and morphology of the heterojunction net were checked, as shown in Fig. 7. The diffraction peaks of Cu, Cu$_2$O, and CuO were clearly observed in the XRD spectra (Fig. 7a), indicating the same compositions of the heterojunction as the sample before photocatalysis. Additionally, no damage was caused to the heterojunction morphology during the photocatalysis procedure. Dense CuO nanowire arrays were well retained on the net surface (Fig. 7b). A small quantity of particles observed on the
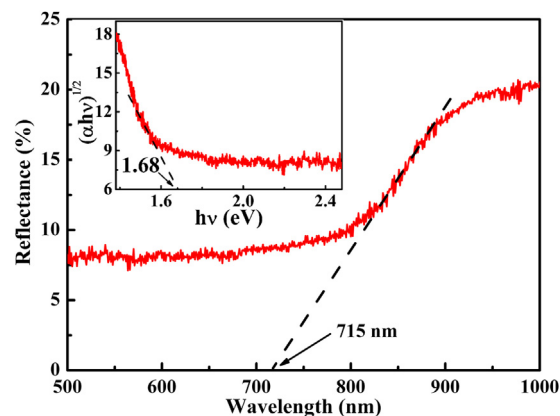

Fig. 5. (a) UV–vis diffuse reflectance spectra of the Cu/Cu$_2$O/CuO heterojunction. Tauc plot of Cu/Cu$_2$O/CuO (inset).
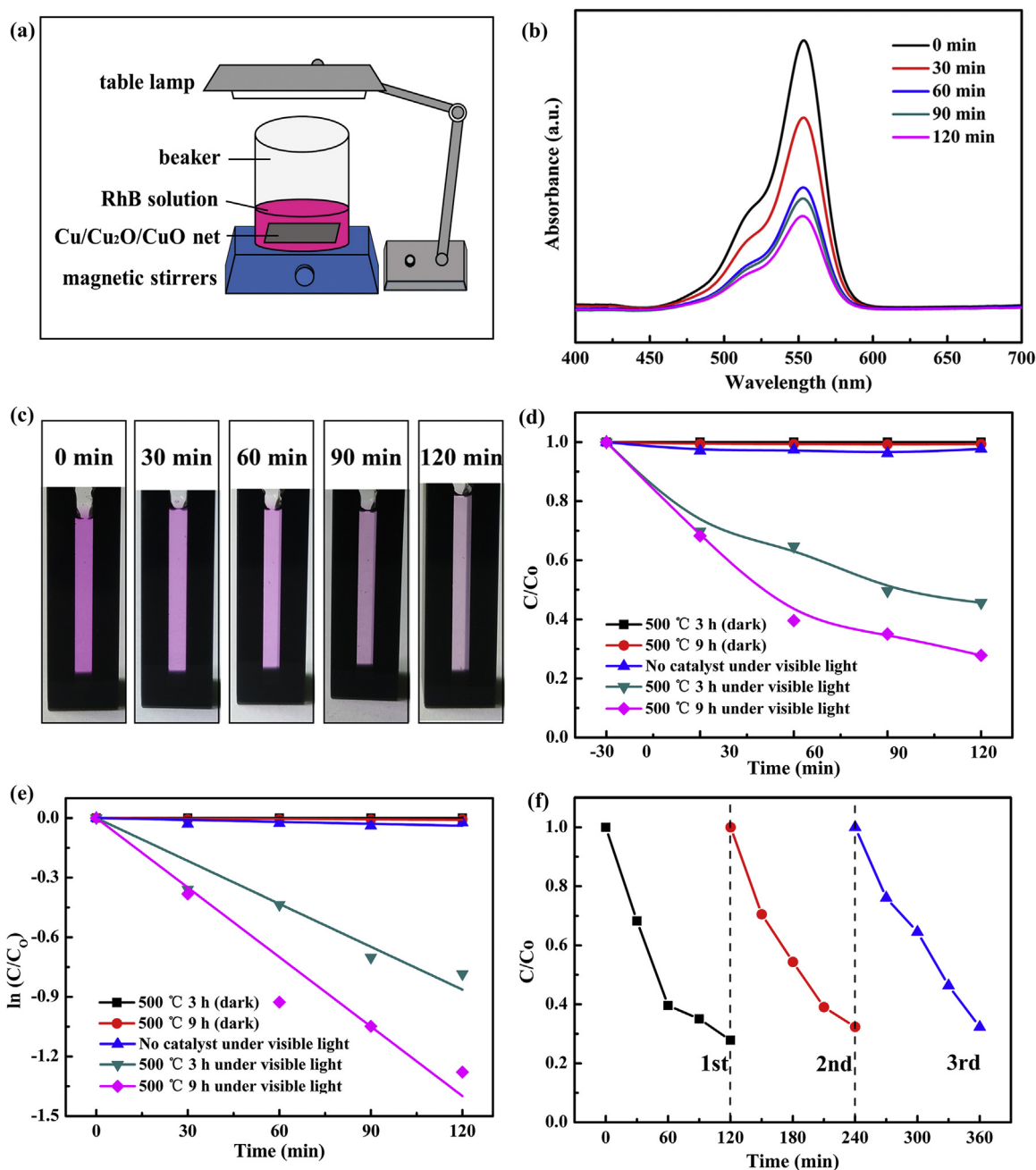
Fig. 6. (a) Schematic illustration of the setup for photocatalytic tests. (b) absorption spectra of RhB and (c) the digital photograph of RhB solution after photocatalysis. (d) degradation profiles of RhB in the presence of catalyst annealed for 3 h and 9 h. (e) the visible-light degradation rate constant for the catalyst annealed for 3 h and 9 h. (f) the photocatalysis repeatability tests of the Cu/Cu$_2$O/CuO heterojunction net.

nanowires might be the adsorbates introduced in the photocatalysis cycles (Fig. 7c). Fig. 7d–e show the Cu XPS and Auger spectrum of Cu/Cu$_2$O/CuO after photocatalysis. The peaks located at 568.2, 568.5 and 569.5 eV in Fig. 7e were respectively ascribed to Cu, Cu^{2+} and Cu$^+$ [41,42], which further confirmed the existence of Cu, CuO, and Cu$_2$O in the heterojunction after the photocatalysis cycles. As shown in Fig. 7d, in comparison with the heterojunction before photocatalysis, the relative percentage of Cu^{2+} (located at 934.7 eV) slightly increased by 6% after photocatalytic degradation, which might result from the oxidation of Cu$^+$ during the photocatalysis processes. The corresponding O1 s XPS spectrum were displayed in Fig. 7f. The oxygen belonging to surface hydroxyl group (located at 531.6 eV [44]) clearly increased, due to the introduced adsorbates on the heterojunction surface in photocatalytic degradation proce-

dure. The good maintenance of both structure and morphology for Cu/Cu$_2$O/CuO heterojunction net in photocatalysis is very favorable for its repeatable use.

The photocatalytic mechanism for the Cu/Cu$_2$O/CuO heterojunction net was proposed based on the band structure, as schematically displayed in Fig. 8. According to the literatures [48,49], the band gaps of free Cu$_2$O and CuO are 2.2 eV and 1.7 eV, respectively. Therefore, both oxides have a wide absorption band in the visible region, and can generate electrons and holes under visible light irradiation. The photoexcited charge carrier transfer direction depends on the band edge positions of the neighbouring materials [24,50]. The reported conduction band (CB) and valence band (VB) edges for Cu$_2$O are −0.28 V vs. the normal hydrogen electrode (NHE) and +1.92 V vs. NHE, and those for CuO are
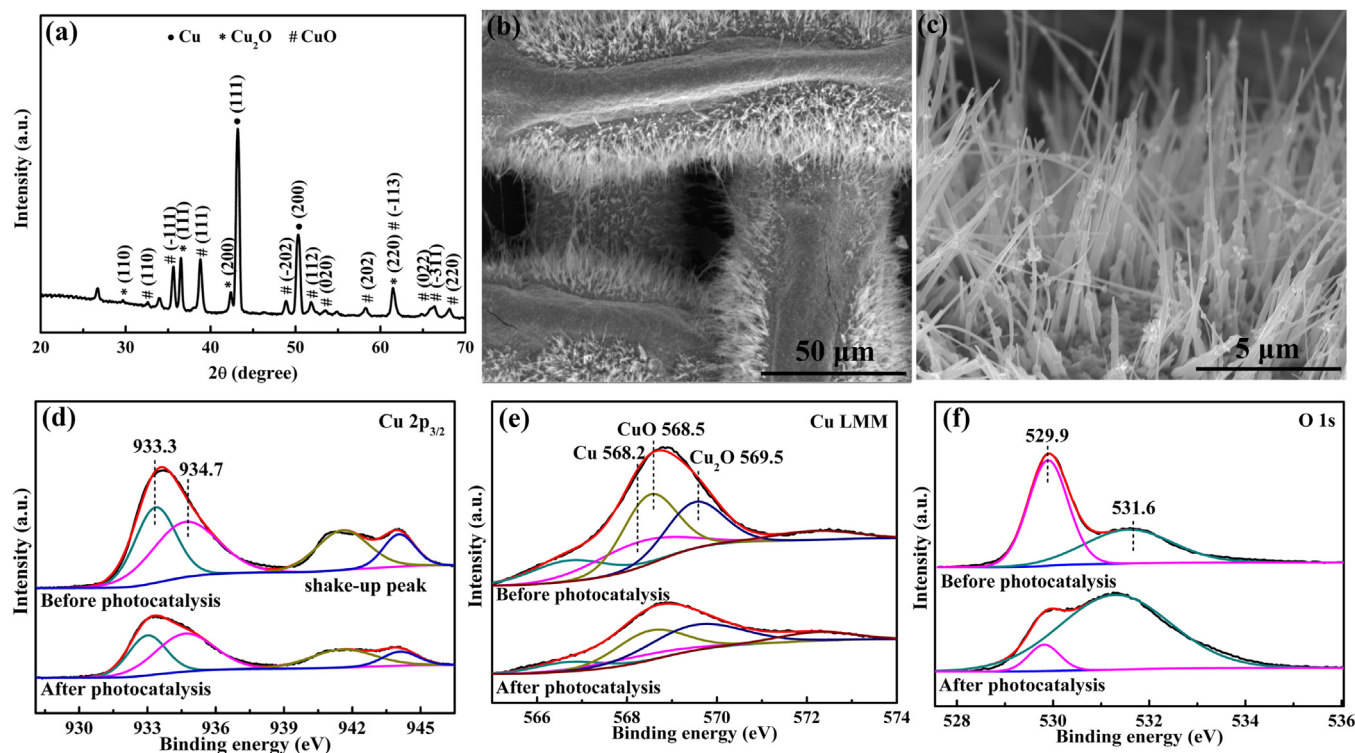
Fig. 7. (a) XRD pattern and (b, c) SEM images of the Cu/Cu$_2$O/CuO heterojunction after three-cycle photocatalysis tests. (d) Cu 2p$_{3/2}$ XPS spectra. (e) Auger spectra of Cu. (f) O 1 s XPS spectra.
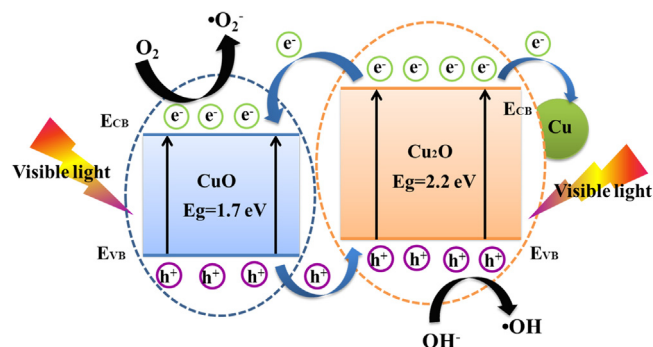

Fig. 8. Proposed schematic illustration of the band structure related photocatalytic mechanism for the Cu/Cu$_2$O/CuO heterojunction net.

+0.46 V *vs.* NHE and +2.16 V *vs.* NHE [48]. Since both CB and VB of Cu$_2$O are situated below those of CuO, the photoexcited electrons from Cu$_2$O transfer to the CB of CuO under visible light irradiation, whereas the photoexcited holes from CuO transfer to the VB of Cu$_2$O [29]. Moreover, with excellent conductivity, Cu framework also acts as good electron acceptors, accepting the photoexcited electrons from CB of Cu$_2$O [50]. Therefore, the photoexcited electrons and holes from the Cu/Cu$_2$O/CuO heterojunction could be efficiently transferred and separated, resulting in a significant increase in their life time. Once the electrons were captured by the adsorbed oxygen molecules and the holes were trapped by the surface hydroxyl, highly oxidative radical species (·O$_2$$^-$ and ·OH) were accordingly generated. The abundant oxidative radical species could accelerate the photocatalysis, leading to the rapid degradation of RhB. Accordingly, the mixing narrow band gaps of the Cu/Cu$_2$O/CuO heterojunction lead to markedly improved visible light photocatalytic activity and consequently ensure its application as photocatalyst.

The multiple-phase heterojunction photocatalysts have been on the spotlight in recent years because of their peculiar structure and

thereupon enhanced visible-light photocatalytic activity. A wide range of materials have been exploited as photocatalysts such as Ag/AgBr/AgVO$_4$ [14], Ag/AgCl/BiVO$_4$ [15], Bi$_7$O$_9$I$_3$/AgI/AgIO$_3$ [18], and Ag$_2$O/Ag$_3$VO$_4$/AgVO$_3$ [19]. Despite these advances achieved, however, the recovery of the catalysts has been a great challenge due to their powder and/or nanoparticle shape. In the circumstances, the water still suffered from an undesirable secondary pollution after photocatalysis treating [51]. Hence, developing easily recycled photocatalysts is an urgent need for water purification. Herein, the fabricated Cu/Cu$_2$O/CuO heterojunction net possessed exceptional free-standing and flexible characteristics, which made its recovery much easier. As seen in Fig. 9, the resulted Cu/Cu$_2$O/CuO heterojunction net had a flexible structure that could be bent without any damage. This flexible property was attributed to the Cu framework of the Cu/Cu$_2$O/CuO heterojunction net. The achievement of free-standing and flexible property enabled it to be facilely separated from the purified water. More importantly, the Cu/Cu$_2$O/CuO heterojunction net was still flexible even after the photocatalysis tests, which provide the possibility of recycling and reuse for this photocatalyst. The free-standing and flexible Cu/Cu$_2$O/CuO photocatalyst developed here may pave a new way for solving the recovery issue of the conventional photocatalysts.

4. Conclusions

In summary, we have developed a simple and fast strategy to fabricate Cu/Cu$_2$O/CuO heterojunction net as a new type of easily recycled visible-light catalysts. This novel heterojunction photocatalyst was composed of a large number of CuO nanowires growing on the Cu@Cu$_2$O core-shell framework surface. The high specific surface area and mixing narrow band gaps of the heterojunction ensured its remarkable visible-light photocatalytic activity, due to the wide absorption band in the visible region and effective electron/hole separation. Moreover, the Cu/Cu$_2$O/CuO heterojunction net exhibited good recycling stability with its composition and
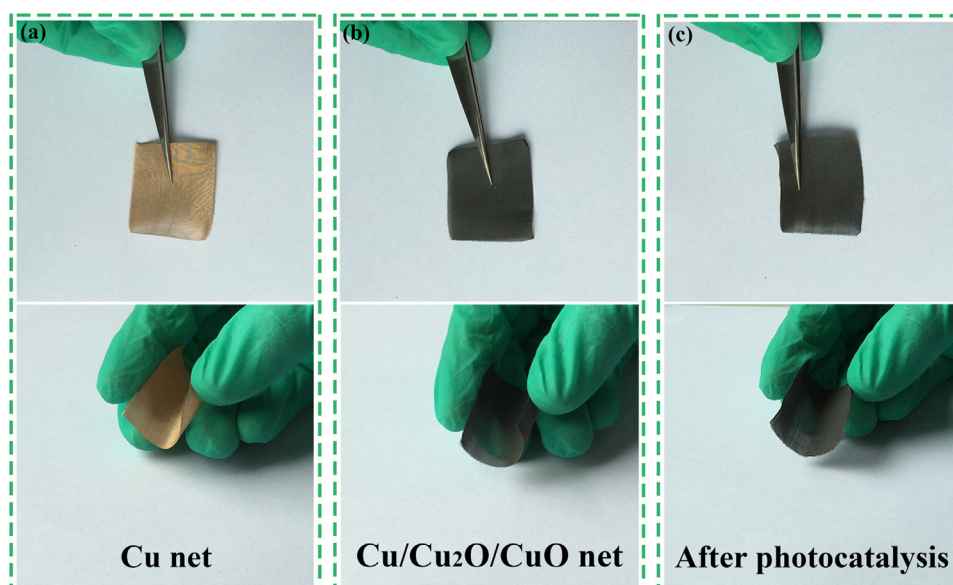
Fig. 9. The digital photographs showing the excellent flexible characteristic of the samples: (a) a Cu net; (b) a Cu/Cu₂O/CuO net; and (c) the Cu/Cu₂O/CuO net after photocatalysis.

morphology well retained after photocatalysis. In comparison with the previously reported photocatalysts fabricated by tedious fabrication processes, the Cu/Cu$_2$O/CuO heterojunction was obtained by one-step calcination in air, which was relatively convenient with high throughput. Unlike the conventional powder and/or nanoparticle photocatalysts, free-standing and flexible property was achieved in Cu/Cu$_2$O/CuO for the first time, which enabled its recovery much easier and solved a key issue for practical applications of the photocatalysts. With advantages of low cost, facile fabrication, visible-light response, together with flexible characteristic, this newly developed Cu/Cu$_2$O/CuO heterojunction net is anticipated to be a highly promising photocatalyst that can serve in broad applications.

Acknowledgments

Appendix A. Supplementary data

Supplementary data associated with this article can be found, in the online version, at http://dx.doi.org/10.1016/j.apcatb.2017.02.013.

References

[1] M.N. Chong, B. Jin, C.W. Chow, C. Saint, Recent developments in photocatalytic water treatment technology: a review, Water Res. 44 (2010) 2997–3027.

[2] C.B. Marien, T. Cottinea, D. Robert, P. Drogui, TiO$_2$ nanotube arrays: influence of tube length on the photocatalytic degradation of paraquat, Appl. Catal. B: Environ. 194 (2016) 1–6.

[3] W.K. Jo, S. Kumar, M.A. Isaacs, A.F. Lee, S. Karthikeyan, Cobalt promoted TiO$_2$/GO for the photocatalytic degradation of oxytetracycline and congo red, Appl. Catal. B: Environ. 201 (2017) 159–168.

[4] S.U. Khan, M. Al-Shahry, W.B. Ingler, Efficient photochemical water splitting by a chemically modified n-TiO$_2$, Science 297 (2002) 2243–2245.

[5] D. Li, H. Haneda, S. Hishita, N. Ohashi, Visible-light-driven N-F-codoped TiO$_2$ photocatalysts: optical characterization, photocatalysis, and potential application to air purification, Chem. Mater. 17 (2005) 2596–2602.

[6] N. Patel, R. Jaiswal, T. Warang, G. Scarduelli, A. Dashora, B. Ahuja, D. Kothari, A. Miotello, Efficient photocatalytic degradation of organic water pollutants using V-N-codoped TiO$_2$ thin films, Appl. Catal. B: Environ. 150–151 (2014) 74–81.

[7] M. Sakar, S. Balakumar, P. Saravananb, S. Bharathkumara, Particulates vs. fibers: dimension featured magnetic and visible light driven photocatalytic properties of Sc modified multiferroic bismuth ferrite nanostructures, Nanoscale 8 (2016) 1147–1160.

[8] Y. Shimodaira, H. Kato, H. Kobayashi, A. Kudo, Photophysical properties and photocatalytic activities of bismuth molybdates under visible light irradiation, J. Phys. Chem. B. 110 (2006) 17790–17797.

[9] L. Zhang, H. Wang, Z. Chen, P.K. Wong, J. Liu, Bi$_2$WO$_6$ micro/nano-structures: synthesis modifications and visible-light-driven photocatalytic applications, Appl. Catal. B: Environ. 106 (2011) 1–13.

[10] J. Cheng, J. Feng, W. Pan, Enhanced photocatalytic activity in electrospun bismuth vanadate nanofibers with phase junction, ACS Appl. Mater. Interfaces. 7 (2015) 9638–9644.

[11] Q. Wang, L. Yuan, M. Dun, X. Yang, H. Chen, J. Li, J. Hu, Synthesis and characterization of visible light responsive Bi$_3$NbO$_7$ porous nanosheets photocatalyst, Appl. Catal. B: Environ. 196 (2016) 127–134.

[12] N. Tian, Y. Zhang, H. Huang, Y. He, Y. Guo, Influences of Gd substitution on the srystal structure and visible light-driven photocatalytic performance of Bi$_2$WO$_6$, J. Phys. Chem. C 118 (2014) 15640–15648.

[13] X. Li, J. Yu, M. Jaroniec, Hierarchical photocatalysts, Chem. Soc. Rev. 45 (2016) 2603–2636.

[14] Q. Zhu, W.S. Wang, L. Lin, G.Q. Gao, H.L. Guo, H. Du, A.W. Xu, Facile synthesis of the novel Ag$_3$VO$_4$/AgBr/Ag plasmonic photocatalyst with enhanced photocatalytic activity and stability, J. Phys. Chem. C 117 (2013) 5894–5900.

[15] R. Qiao, M. Mao, E. Hu, Y. Zhong, J. Ning, Y. Hu, Facile formation of mesoporous BiVO$_4$/Ag/AgCl heterostructured microspheres with enhanced visible-light photoactivity, Inorg. Chem. 54 (2015) 9033–9039.

[16] S. Zhang, J. Li, X. Wang, Y. Huang, M. Zeng, J. Xu, In situ ion exchange synthesis of strongly coupled Ag@AgCl/g-C$_3$N$_4$ porous nanosheets as plasmonic photocatalyst for highly efficient visible-light photocatalysis, ACS Appl. Mater. Interfaces 6 (2014) 22116–22125.

[17] X. Yang, Z. Chen, J. Xu, H. Tang, K. Chen, Y. Jiang, Tuning the morphology of g-C$_3$N$_4$ for improvement of z-scheme photocatalytic water oxidation, ACS Appl. Mater. Interfaces 7 (2015) 15285–15293.

[18] C. Zeng, Y. Hu, Y. Guo, T. Zhang, F. Dong, X. Du, Y. Zhang, H. Huang, Achieving tunable photocatalytic activity enhancement by elaborately engineering composition-adjustable polynary heterojunctions photocatalysts, Appl. Catal. B: Environ. 194 (2016) 62–73.

[19] R. Ran, X. Meng, Z. Zhang, Facile preparation of novel graphene oxide-modified Ag$_2$O/Ag$_3$VO$_4$/AgVO$_3$ composites with high photocatalytic activities under visible light irradiation, Appl. Catal. B: Environ. 196 (2016) 1–15.

[20] Y. Huang, S. Kang, Y. Yang, H. Qin, Z. Ni, S. Yang, X. Li, Facile synthesis of Bi/Bi$_2$WO6 nanocomposite with enhanced photocatalytic activity under visible light, Appl. Catal. B: Environ. 196 (2016) 89–99.

[21] J. Esmaili-Hafshejani, A. Nezamzadeh-Ejhieh, Increased photocatalytic activity of Zn(II)/Cu(II) oxides and sulfides by coupling and supporting them onto clinoptilolite nanoparticles in the degradation of benzophenone aqueous solution, J. Hazard. Mater. 316 (2016) 194–203.

[22] H. Moussa, E. Giro, K. Mozet, H. Alem, G. Medjahdi, R. Schneider, ZnO rods/reduced graphene oxide composites prepared via a solvothermal reaction for efficient sunlight-driven photocatalysis, Appl. Catal. B: Environ. 185 (2016) 11–21.

[23] Y. Fan, W. Ma, D. Han, S. Gan, X. Dong, L. Niu, Convenient recycling of 3D AgX/graphene aerogels (X = Br, Cl) for effi cient photocatalytic degradation of water pollutants, Adv. Mater. 27 (2015) 3767–3773.

[24] Q. Zhang, K. Zhang, D. Xu, G. Yang, H. Huang, F. Nie, C. Liu, S. Yang, CuO nanostructures: synthesis, characterization, growth mechanisms, fundamental properties, and applications, Prog. Mater. Sci. 60 (2014) 208–337.

[25] B.K. Meyer, A. Polity, D. Reppin, M. Becker, P. Hering, P.J. Klar, T. Sander, C. Reindl, J. Benz, M. Eickhoff, C. Heiliger, M. Heinemann, J. Blasing, S. Krost, C. Muller, C. Ronning, Binary copper oxide semiconductors: from materials towards devices, Phys. Status Solidi B 249 (2012) 1487–1509.

[26] E. Guo, L. Yin, Nitrogen doped TiO_2-Cu_xO core-shell mesoporous sphere hybrids for high-performance dye-sensitized solar cells, Phys. Chem. Chem. Phys. 17 (2015) 563–574.

[27] Z. Wang, Y. Liu, D.J. Martin, W. Wang, J. Tang, W. Huang, CuO_x-TiO_2 junction: what is the active component for photocatalytic H_2 production, Phys. Chem. Chem. Phys. 15 (2013) 14956–14960.

[28] Z. Zhang, K. Liu, Y. Bao, B. Dong, Photo-assisted self-optimizing of charge-carriers transport channel in the recrystallized multi-heterojunction nanofibers for highly efficient photocatalytic H_2 generation, Appl. Catal. B: Environ. 203 (2017) 599–606.

[29] Y. Yang, D. Xu, Q. Wu, P. Diao, Cu_2O/CuO bilayered composite as a high-efficiency photocathode for photoelectrochemical hydrogen evolution reaction, Sci. Rep. 6 (2016) 35158.

[30] M. Prathap, B. Kaur, R. Srivastava, Hydrothermal synthesis of CuO micro-/nanostructures and their applications in the oxidative degradation of methylene blue and non-enzymatic sensing of glucose/H_2O_2, J. Colloid. Interface. Sci. 370 (2012) 144–154.

[31] H. Xu, G. Zhu, D. Zheng, C. Xi, X. Xu, X. Shen, Porous CuO superstructure: precursor-mediated fabrication, gas sensing and photocatalytic properties, J. Colloid. Interface. Sci. 383 (2012) 75–81.

[32] S. Zaman, A. Zainelabdin, G. Amin, O. Nur, M. Willander, Efficient catalytic effect of CuO nanostructures on the degradation of organic dyes, J. Phys. Chem. Solids 73 (2012) 1320–1325.

[33] S. Liu, J. Tian, L. Wang, Y. Luo, X. Sun, One-pot synthesis of CuO nanoflower-decorated reduced graphene oxide and its application to photocatalytic degradation of dyes, Catal. Sci. Technol. 2 (2012) 339–344.

[34] W. Shi, N. Chopra, Controlled fabrication of photoactive copper oxide–cobalt oxide nanowire heterostructures for efficient phenol photodegradation, ACS Appl. Mater. Interfaces 4 (2012) 5590–5607.

[35] X. Jiang, T. Herricks, Y. Xia, CuO nanowires can be synthesized by heating copper substrates in air, Nano Lett. 2 (2002) 1333–1338.

[36] M. Kaura, K. Muthe, S. Despande, S. Choudury, J. Singh, N. Verma, S. Gupta, J. Yakhmi, Growth and branching of CuO nanowires by thermal oxidation of copper, J. Cryst. Growth. 289 (2006) 670–675.

[37] M. Yin, C.-K. Wu, Y. Lou, C. Burda, J.T. Koberstein, Y. Zhu, S.O. Brien, Copper oxide nanocrystals, J. Am. Chem. Soc. 127 (2005) 9506–9511.

[38] K.V.R. Chary, G.V. Sagar, C.S. Srikanth, V.V. Rao, Characterization and catalytic functionalities of copper oxide catalysts supported on zirconia, J. Phys. Chem. B 111 (2007) 543–550.

[39] R. Bechara, A. Aboukais, J.-P. Bonnelle, X-ray photoelectron spectroscopic study of a Cu-Al-O catalyst under H_2 or CO atmospheres, J. Chem. Soc. Faraday Trans. 89 (1993) 1257–1262.

[40] D.R. Kumar, D. Manoj, J. Santhanalakshmi, Optimization of site specific adsorption of oleylamine capped CuO nanoparticles on MWCNTs for electrochemical determination of guanosine, Sens. Actuators B 188 (2013) 603–612.

[41] P. Liu, E.J.M. Hensen, Highly efficient and robust Au/MgCuCr2O4 catalyst for gas-phase oxidation of ethanol to acetaldehyde, J. Am. Chem. Soc. 135 (2013) 14032–14035.

[42] I. Platzman, R. Brener, H. Haick, R. Tannenbaum, Oxidation of polycrystalline copper thin films at ambient conditions, J. Phys. Chem. C 112 (2008) 1101–1108.

[43] G. Du, X. Liu, Y. Zong, T.A. Hor, A. Yu, Z. Liu, Co_3O_4 nanoparticle-modified MnO_2 nanotube bifunctional oxygen cathode catalysts for rechargeable zinc-air batteries, Nanoscale 5 (2013) 4657–4661.

[44] H. Chen, M. Zhou, T. Wang, F. Li, Y.X. Zhang, Construction of unique cupric oxide-manganese dioxide core-shell arrays on a copper grid for high-performance supercapacitors, J. Mater. Chem. A 4 (2016) 10786–10793.

[45] A. Al-keisy, L. Ren, D. Cui, Z. Xu, X. Xu, X. Su, W. Hao, S.X. Dou, Y. Du, A ferroelectric photocatalyst $Ag_{10}Si_4O_{13}$ with visible-light photo-oxidation properties, J. Mater. Chem. A 4 (2016) 10992–10999.

[46] J. Tauc, R. Grigorovici, A. Vancu, Optical properties and electronic structure of amorphous germanium, Phys. Status. Solidi. B 15 (1966) 627–637.

[47] J. Xiao, Y. Xie, F. Nawaz, S. Jin, F. Duan, M. Li a, H. Cao, Super synergy between photocatalysis and ozonation using bulk g-C_3N_4 as catalyst: a potential sunlight/O_3/g-C_3N_4 method for efficient water decontamination, Appl. Catal. B: Environ. 181 (2016) 420–428.

[48] Y. Xu, M.A.A. Schoonen, The absolute energy positions of conduction and valence bands of selected semiconducting minerals, Am. Mineral 85 (2000) 543–556.

[49] M. Heinemann, B. Eifert, C. Heiliger, Band structure and phase stability of the copper oxides Cu_2O CuO, and Cu_4O_3, Phys. Rev. B. 87 (2013) 115111.

[50] T. Liu, B. Liu, L. Yang, X. Ma, H. Li, S. Yin, T. Sato, T. Sekino, Y. Wang, RGO/Ag_2S/TiO_2 ternary heterojunctions with highly enhanced UV-NIR photocatalytic activity and stability, Appl. Catal. B: Environ. 204 (2017) 593–601.

[51] T.L. Su, C.S. Chiou, H.W. Chen, Preparation photocatalytic activity, and recovery of magnetic photocatalyst for decomposition of benzoic acid, In. J. Photoenergy 2012 (2012) 1–8.